Synthesis, magnetic properties and theoretical calculations of novel nitronyl nitroxide and imino nitroxide diradicals grafted on terpyridine moiety

ARTICLE *in* POLYHEDRON · JULY 2003

Impact Factor: 2.01 · DOI: 10.1016/S0277-5387(03)00258-4 · Source: OAI

Available online at www.sciencedirect.com
SCIENCE DIRECT®
PERGAMON
Polyhedron 22 (2003) 2099–2110
POLYHEDRON
www.elsevier.com/locate/poly

Synthesis, magnetic properties and theoretical calculations of novel nitronyl nitroxide and imino nitroxide diradicals grafted on terpyridine moiety

Giorgio Zoppellaro, Anela Ivanova, Volker Enkelmann, Ahmed Geies, Martin Baumgarten *

Max Planck Institute for Polymer Research, Ackermannweg 10, D-55128 Mainz, Germany

Received 6 October 2002; accepted 2 January 2003

Abstract

The synthetic route based on Stille coupling between tributyltinpyridyl derivatives and bromo substituted mono- and dipyridylcarbaldehyde is used for the synthesis of 5,5″-diformyl-2,2′:6′,2″-terpyridine (**8**). A sequence of Ullman coupling with 2,3-bis(hydroxylamino)-2,3-dimethylbutane followed by oxidation under phase transfer conditions affords either 5,5″-Bis(1-oxyl-3-oxo-4,4,5,5-tetramethylimidazolidin-2-yl)2,2′:6′,2″-terpyridine (**10**) (diNN-Terpy) or the related 5,5″-Bis(1-oxyl-4,4,5,5-tetramethylimidazolidin-2-yl)2,2′:6′,2″-terpyridine (**11**) (diIN-Terpy), where both biradicals display clear intramolecular ferromagnetic interaction between the single spin units as evidenced by ESR spectroscopy. Quantum chemical calculations (ROHF/AM1) are performed showing the triplet ground-state for both **10** and **11** radicals.

Keywords: Terpyridine; Organic based magnets; EPR radicals; Open-shell molecules; Nitronyl nitroxide; Semiempirical (AM1) calculations

1. Introduction

There is growing interest in developing novel synthetic routes for functionalized 2,2′:6′,2″-terpyridines [1a] due to their rich coordination chemistry [1b,1c], for supramolecular assembly [2], in molecular biology [3] and even in photochemistry [4]. In addition much attention has been devoted over the last decade to develop different sets of molecular units carrying either free radicals or luminophoric centers for use as novel magnetic materials or optical devices [5]. In that vein terpyridine based radicals offer both advantages, although relatively few examples of those are available up to now in literature [6]. Since the discovery of nitronyl nitroxide (NIT) by Ullman [7] this class of radicals was widely used as building block constituents for the preparation of molecular based magnets, due to their exceptional stability, facile preparation, versatility in coordination properties and ability to generate cooperative magnetic properties [8]. In the nitronyl nitroxide radical the spin density of the unpaired electron is delocalized over two sites of coordination, leaving open the possibility to arrange the molecular unit into a supramolecular network. This assumption may be regarded as the '*condicio sine qua non*' to achieve high Curie-temperatures (T_c) below which materials behave like magnets [9]. In fact the first example of pure organic ferromagnets is based on the β-phase of *p*-nitrophenyl-nitronyl nitroxide radical with $T_c = 0.64$ K [10]. Thus the first point to consider in designing novel organic-based magnets, if more than one radical unit is connected through a spacer or coupling unit, is the clear

* Corresponding author. Tel.: +49-6131-37-9142; fax: +49-6131-37-9370.
E-mail address: baumgart@mpip-mainz.mpg.de (M. Baumgarten).

0277-5387/03/$ - see front matter
doi:10.1016/S0277-5387(03)00258-4

understanding of the intramolecular exchange interaction (J) between the radical fragments, prior to their possible use as novel building blocks in a supramolecular network. Different models, that serve as general guide-line in the design, have been proposed so far to describe and predict the ground spin-state of non-Kekulé hydrocarbons [11] in such way that, by controlling the connectivity between the paramagnetic fragments (topological model), the conjugated coupler provides path and signs for the exchange interaction (J). To best of our knowledge no terpyridine ligands bearing two Ullman radicals in position 5-5″ were synthesized so far. In order to justify the synthetic effort, two considerations were finally taken into account. First to test the 'topological prediction', where radicals attached in position 5-5″ should ferromagnetically interact through the terpyridine moiety and second to account for the observation that metal-complexation of terminally substituted terpyridine sometimes proceeds better if the substituents are in position 5-5″ rather than in others [12], thus leaving open the possibility to build more easily hybrid inorganic–organic magnetic materials. Here we fill the gap by reporting the synthesis of 5,5″-Bis(1-oxyl-3-oxo-4,4,5,5-tetramethylimidazolidin-2-yl)2,2′:6′,2″-terpyridines (**10**) and the related 5,5″-Bis(1-oxyl-4,4,5,5-tetramethylimidazolidin-2-yl)2,2′:6′,2″-terpyridines (**11**) where intramolecular ferromagnetic interaction between the single spin units was disclosed and analyzed by EPR spectroscopy (from RT down to 4 K). In addition quantum chemical calculations have been performed showing the triplet ground-state for both radicals **10** and **11**, in agreement with the topological prediction.

2. Experimental

2.1. General methods

Solvents were distilled before use and kept dry over molecular sieves; in particular diethylether and toluene were dried over sodium/benzophenone and distilled under Argon. All the reagents were used as received. 2,5-Dibromopyridine (**1**), 2,6-dibromopyridine (**5**), Bis-(triphenylphosphine)-palladium(II)-chloride $[(C_6H_5)_3P]_2PdCl_2$ (98%), triphenylphosphine $[(C_6H_5)_3P]$, and 2,3-dimethyl-2,3-dinitrobutane (98%) were purchased from Aldrich. Toluene-4-sulfonic-acid ($CH_3C_6H_4SO_3H\cdot H_2O$), tributyltin chloride (Bu_3SnCl, 97%), Aluminium oxide (type 507 C neutral, 0.05–0.015 mm) were purchased by Fluka. n-BuLi (1.6 M in hexane) was purchased from Across Organics. ESR spectra were recorded in diluted and degassed solution of toluene with the concentration of 1×10^{-4} mol dm^{-3} unless otherwise stated by using a Bruker X-band spectrometer ESP300 E, equipped with an NMR gaussmeter (Bruker ER035), a frequency counter (Bruker ER 041 XK) and a variable temperature control continuous flow N_2 cryostat (Bruker B-VT 2000) or with Oxford system (ESR 910) helium continuos flow cryostat. The g-factor corrections were achieved by using PNT radical ($g = 2.0026$) or DPPH ($g = 2.0037$) as standard. UV–Vis spectra were recorded in $CHCl_3$ solutions with Perkin Elmer Spectrometer (UV/Vis/NIR Lambda 900) by using 1 cm optical-path quartz cell at room temperature. ^{1}H and ^{13}C NMR spectra were recorded on Bruker AMX 250 spectrometer. IR spectra were recorded in KBr pellet (Nicolet 730 FT-IR Spectrometer) at room temperature. Mass spectra were obtained on FD MS, VG Instruments ZAB-2 mass spectrometer (FAB, positive mode, m-nitrobenzyl-alcohol as matrix). Elemental analyses were performed at the University of Mainz, Faculty of Chemistry and Pharmacy. Melting points were measured on Büchi B-545 apparatus (uncorrected). Although **2** (6-bromo-3-pyridinecarbaldehyde) was previously prepared by selective mono-lithiation [14], no complete synthetic procedures for **2** were reported [15]; in addition **6** was prepared using adapted literature procedures [16] and 2,3-bis-hydroxylamino-2,3 dimethylbutane (free base) was prepared according to the procedure of Ovcharenko et al. [20].

2.2. Computational studies

A semi-empirical (ROHF/AM1) approach with extended configuration interaction (CAS) was used for assessing the spin-state ordering of each biradical. The active space involved mixing of 8 electrons in 8 MOs, i.e. CAS [8,8]. This CAS choice was largely dictated by the nature of the frontier MOs; whereas the next-larger MO active space is not admissible due to orbital degeneracy, further extensions are already impracticable from a computational perspective. The CAS method provides the only size-consistent treatment of the lowest spin-dependent states. In the computation of local spin densities however, we expand substantially the MO basis at the expense of dropping the CAS requirement. Namely, we use the single-excited CI approach for 20 electrons in 20 MOs, or CIS [20,20]. The semi-empirical computations were performed with an upgraded version of MOPAC [21,22].

2.3. Synthesis of 6-bromo-3-pyridinecarbaldehyde (2)

The 2,5-dibromopyridine (**1**, 5 g, 21.1 mmol) was charged into a flask, evacuated and kept under argon. Dry diethylether (130 ml) was added from a syringe under stirring and the solution was cooled to −78 °C in dry ice/acetone bath. The yellowish solution appears very dense due to the low solubility of **1** in diethyl ether at this concentration (0.144 M). Then n-BuLi (1.6 M in

hexane, 16 ml, 25.3 mmol) was added drop-wise from a syringe within 10 min. As soon as the addition was completed, the color of the dense solution turned into red. The reaction mixture was stirred for 35 min under continuous cooling, then dry *N*-*N*-dimethylformamide (DMF) (2.3 ml, 29.5 mmol, $d = 0.94$ g ml^{-1}) was added drop-wise within 5 min. The solution turned into deep clear red. The temperature (−78 °C) was maintained further for 90 min and after that raised slowly till −35 °C and kept for additional 30 min at this temperature. Then the solution was warmed to room temperature. A saturated solution of ammonium chloride (50 ml) was added and the mixture was shaken vigorously in a separator funnel. The phases were separated and the aqueous layer was extracted with dichloromethane (3 × 30 ml). The combined organic layers were collected and the solvent evaporated under reduced pressure to a small volume. The crude oily mixture was then separated by column chromatography (silica gel, dichloromethane/hexane, 3/2). The main isolated product was 6-bromo-3-pyridinecarbaldehyde (**2**) ($R_f = 0.26$) as pale yellow powder. The product was finally washed with small cold portions of light petroleum ether (3 × 15 ml) (b.p. 30–40 °C) and **2** was collected as highly pure white crystalline powder (2.63 g, 67%). Starting from 10 g of **1** we obtain 4.32 g of pure **2** (yield 55%). M.p. 97–98 °C (lit. 100 °C, [24]), ^{1}H NMR ($CDCl_3$, 250 MHz) 10.03 δ (s, 1H, –CHO), 8.77 δ (s, 1H, H-6), 7.94 δ (d, 1H, $J =$ 8.2 Hz, H-4), 7.62 δ (d, 1H, $J = 8.1$ Hz, H-3). ^{13}C NMR ($CDCl_3$, 63 MHz, δ ppm) 189.85, 152.88, 148.66, 137.87, 130.95, 129.38. MS FD (70 eV) 187.2 (100%) (MW+H calculated 187.01). UV–Vis ($CHCl_3$, ε M^{-1} cm^{-1}) 282 nm (24560), 310 nm (2860), 321 nm (2060).

2.4. Synthesis of 2-bromo-5-[1,3]dioxolan-2-yl-pyridine (*3*)

The 6-bromo-3-pyridinecarbaldehyde (**2**, 1 g, 5.37 mmol) was charged into a round flask together with benzene (30 ml), ethyleneglycol (0.54 ml, 9.7 mmol) and para-toluene-sulfonic-acid as catalyst (0.08 g, 0.42 mmol, 8% with respect to **2**). The solution was heated to reflux and stirred for one day. Then it was neutralized with diluted aqueous potassium carbonate (K_2CO_3) till pH 8–9 and the phases were separated. The aqueous layer was extracted with small portions of benzene (3 × 10 ml) and the combined organic layers were collected, dried over $MgSO_4$ and filtered. The benzene solution was evaporated under reduced pressure and the resulting oil was dried in vacuum overnight at 40 °C. Totally 1.086 g (4.7 mmol) of 2-bromo-5-[1,3]dioxolan-2-yl-pyridine (**3**) as pale yellow oil was obtained (yield 87%). B.p. >200 °C (760 mbar) ^{1}H NMR ($CDCl_3$, 250 MHz) 8.43 δ (s, 1H, H-6), 7.62 δ (dd, 1H, $J = 2.2$, 7.9 Hz, H-3), 7.49 δ (d, 1H, $J = 8.2$ Hz, H-4), 5.80 δ (s, 1H, –CH), 4.32 δ (m, 4H, $-CH_2$). ^{13}C NMR ($CDCl_3$, 63 MHz, δ ppm) 147.7, 141.8, 135.7, 132.1, 126.8, 100.2, 64.4. MS FD (70 eV) 230.1 (100%, M^+), (MW calculated 230.06).

2.5. Synthesis of 2-tributylstannyl-5-[1,3]dioxolan-2-yl-pyridine (*4*)

The 2-bromo-5-[1,3]dioxolan-2-yl-pyridine (**3**, 1.086 g, 4.7 mmol) was charged into a round flask together with freshly distilled diethylether (40 ml), and kept under argon. The solution was cooled to −78 °C using dry ice/acetone bath and *n*-BuLi (1.6 M in hexane, 3.5 ml, 5.7 mmol) was added slowly within 10 min. The mixture was kept for 90 min at this temperature under stirring and rigorous argon atmosphere. Initially, after the complete addition of *n*-BuLi the color of the solution appeared deep-green and after 90 min turned black. Tributyltin-chloride (Bu_3SnCl, 97%) (1.66 ml, 6.2 mmol) was added within 5 min. The solution slowly turned into deep-red. The low temperature (−78 °C) was maintained for 120 min and after that the mixture was allowed to warm up slowly to room temperature overnight. The oily solution was filtered from the inorganic salts and the solvent evaporated under reduced pressure. Finally 3.8 ml of bright orange oil ($d = 1.05$ g ml^{-1}) were obtained and used for the next step without purification.

2.6. Synthesis of 2-tributylstannyl-6-bromopyridine (*6*)

The 2,6-dibromopyridine (**5**, 1g, 4.22 mmol) was charged into a flask, evacuated and put under argon. Dry diethylether (70 ml) was added from a syringe under stirring and the solution was cooled to −50 °C in dry ice/acetone bath. The white solution appears very dense due to the low solubility of **5** in diethylether. Then excess of *n*-BuLi (1.6 M in hexane, 5.6 ml, 8.96 mmol) was added drop-wise from a syringe within 3 min; as soon as the addition was completed the color of the mixture turned into deep green. The reaction mixture was stirred for 30 min under continuous cooling (−50 °C) then the temperature was lowered till −60 °C. Tributhylstannyl-chloride (Bu_3SnCl, 97%) (2.72 ml, 10.1 mmol) was added from a syringe within 5 min. When half of the addition was completed the solution became pale green and very limpid. The temperature was maintained for 60 min, then lowered till −78 °C and kept for an additional hour. Finally the mixture was allowed to warm slowly overnight till room temperature. The solution was filtered from the white inorganic salts and dry toluene (2 ml) was added. The organic solution was collected and the diethylether was evaporated under reduced pressure avoiding heating to afford 3.7 ml of **6** as pale yellowish oil (1.134 g ml^{-1}) which was used in the next step without purification.

2.7. Synthesis of 6-bromo-2,2′-dipyridine-5′-carbaldehyde (7)

The crude oily 2-tributylstannyl-6-bromopyridine (**6**, 3.7 ml, 4.22 mmol) was transferred into a two-necked round bottomed flask together with an excess of 6-bromo-3-pyridinecarbaldehyde (**2**, 1.8 g, 9.7 mmol). The mixture was degassed and kept under argon. Then dry and degassed toluene (70 ml) was added with a syringe together with dichlorobis(triphenylphosphine)-palladium(II) (148 mg, 0.21 mmol, 5% with respect to **6**) and triphenylphosphine (110 mg, 0.42 mmol) as catalyst. The solution was then heated to reflux, in argon under stirring, for 72 h. During the reaction the initially light-yellow solution became very dark after 72 h. The solvent was evaporated under reduced pressure and then dichloromethane (50 ml) together with a saturated solution of ammonium-chloride (30 ml) and a solution of EDTA (5%, 10 ml) were added to the resulting black-slurry. The mixture was shaken vigorously in a separator funnel and the phases were separated. The aqueous layer was extracted with portions of dichloromethane (2×30 ml). The combined organic layers were collected and the solvent evaporated under reduced pressure till small volume. The crude oily mixture was subjected to column chromatography (silica gel, ethyl-acetate/dichloromethane/hexane, 1/3/4). The main fraction eluted was 6-bromo-2,2′-dipyridine-5′-carbaldehyde (**7**) ($R_f = 0.65$) as pale yellow powder. The product was further washed with small cold portions of light petroleum ether (2×5 ml) (b.p. 30–40 °C) and **7** was collected as highly pure white crystalline powder (750 mg, 68%). The second colorless fraction collected was found to consist of [2,2′]-bipyridinyl-5-5′-dicarboxaldehyde ($R_f = 0.25$, 90 mg) as homo-coupled product of **2** [19]. Starting from 8.44 mmol (7.4 ml) of **6** and 3.6 g of **2** (19.4 mmol) we obtain 1.29 g of **7** (yield 58%). ^{1}H NMR ($CDCl_3$, 250 MHz) δ (ppm): 10.15 (s, 1H, –CHO), 9.09 (s, 1H, H-6′), 8.57 (d, $J = 8.5$ Hz, 1H, H-3), 8.45 (d, $J = 7.7$ Hz, 1H, H-3′), 8.28 (d, $J = 8.3$ Hz, 1H, H-4′), 7.70 (t, $J = 7.8$ Hz, 1H, H-4), 7.56 (d, $J = 7.8$ Hz, 1H, H-5). ^{13}C NMR (CDCl3, 63 MHz, δ ppm): 188.7, 157.2, 154.2, 149.8, 140.2, 137.7, 135.4, 129.7, 127.4, 119.9, 119.2. MS FD (70 eV) 264.1 (M-H, 100%), MW calculated (MW + H) 264.1. UV–Vis ($CHCl_3$) λ_{max} (ε, $mol^{-1}cm^{-1}$) 321 nm (21 380), 310 nm (25 850), 260 nm (12 030). FT-IR (KBr pellet, ν cm^{-1}) 3042 (w, ν_{C-Hpyr}), 2962 (w, ν_{C-Hal}), 2883 (w, ν_{C-Hal}), 1682 (s, $\nu_{C=O}$), 1592 (s, pyr), 1546 (s, pyr), 1435(m, pyr), 1369 (m), 1263 (m, pyr), 1209 (m, pyr). M.p. 176–177 °C. Elemental analysis Calc. for $C_{11}H_7N_2O \cdot H_2O$: C 47.00%, H 3.20%, N 9.97%, C/N = 4.71; Found: C 47.20%, H 3.30%, N 10.01%, C/N = 4.72.

2.8. Synthesis of 5,5″-diformyl-2,2′:6′,2″-terpyridine (8)

The crude 2-tributylstannyl-5-[1,3]dioxolan-2-yl-pyridine (**4**, 3.8 ml, 4.7 mmol) was placed in a two-necked round bottomed flask together with the 6-bromo-2,2′-dipyridine-5′-carboxaldehyde (**7**, 900 mg, 3.4 mmol). The mixture was degassed and kept under rigorous argon atmosphere. Then dry and degassed toluene (50 ml) was added with a syringe together with dichlorobis(triphenylphosphine)-palladium(II) (165 mg, 0.235 mmol) and triphenylphosphine (123 mg, 0.47 mmol) as catalyst. The solution was heated to reflux in argon under stirring for 60 h. The resulting dark solution was washed with a saturated solution of ammonium-chloride (20 ml). The mixture was shaken vigorously in a separator funnel. The phases were separated and the aqueous layer was extracted with toluene (2×15 ml). The combined dark yellow organic layers were collected and the solvent evaporated under reduced pressure. The oily solution was then treated with HCl (20 ml, 6N) and was heated to reflux for 6 h under stirring. This ensures for the complete hydrolysis of the dioxolane. Basification with a saturated solution of K_2CO_3 shows the formation of a white flocculate at pH 7–8 that consists mainly of 5,5″-diformyl-2,2′:6′,2″-terpyridine (**8**). The crude product was extracted with dichloromethane ($3 \times$ 40 ml). The organic layers were collected and the solvent evaporated till small volume under reduced pressure. The mixture was separated by column chromatography (silica gel, ethyl-acetate/dichloromethane/hexane, 1/4/4). The first almost colorless fraction eluted was 5,5″-diformyl-2,2′:6′,2″-terpyridine (**8**) ($R_f = 0.2$) as pale yellow powder. The product was further washed with small portions of light petroleum ether (2×10 ml) (b.p. 30–40 °C) and **8** was collected as highly pure white crystalline powder (720 mg, 73%). Our data are consistent with those published in Ref. [13] except for the measured melting point and the IR data (previously not reported): white solid, m.p. 246–247 °C in our case versus m.p. 148–156 °C as previously found. FT-IR (KBr pellet, ν cm^{-1}) 3036 (w, ν_{C-Hpyr}), 2961 (w, ν_{C-Hal}), 2877 (ν_{C-Hal}), 1693 (s, $\nu_{C=O}$), 1591(s, pyr), 1560 (s, pyr), 1482 (w, pyr), 1450 (w, pyr), 1371 (s), 1264 (m, pyr), 1205 (m, pyr). ^{1}H NMR (DMSO d_6, 250 MHz) δ (ppm): 10.19 (s, 2H, –CHO), 9.22 (s, 2H, H-6, H-6″), 8.84 (d, $J = 8.2$ Hz, 2H, H-3, H-3″), 8.62 (d, $J = 7.9$ Hz, 2H, H-3′, H-5′), 8.44 (dd, $J = 2.2$, 8,2 Hz, 2H, H-4, H-4″), 8.24 (t, $J = 7.9$ Hz, 1H, H-4′). ^{13}C NMR (DMSO d_6, 63 MHz, δ ppm): 192.5, 159.3, 154.3, 151.9, 139.5, 137.7, 131.7, 123.2, 121.5. MS FD (70 eV) 290.4 (100%), (MW + H calculated 290.4). UV–Vis ($CHCl_3$) λ_{max} (ε, $mol^{-1}cm^{-1}$) 321 nm (31 800), 312 nm (30 870), 256 nm (23 020).

2.9. Synthesis of 5,5″-Bis(1,3-dihydroxy-4,4,5,5-tetramethylimidazolidin-2-yl)2,2′:6′,2″-terpyridine (9)

The 5,5″-diformyl-2,2′:6′,2″-terpyridine (**8**, 590 mg, 2.04 mmol) was placed in a round bottomed flask together with 2,3-bis-hydroxylamino-2,3-dimethylbu-

tane (906 mg, 6.12 mmol). A mixture of 1,4-dioxane, trichloromethane and methanol (20/15/15 ml) was used as reaction solvents due to the low solubility of **8**. The mixture was then stirred for 7 days under argon at room temperature. The white precipitate 5,5″-Bis(1,3-dihydroxy-4,4,5,5-tetramethylimidazolidin-2-yl)2,2′:6′,2″-terpyridine (**9**) was filtered, washed with small portions of cold methanol/acetone (4/1, 3 × 5 ml) and dried in high-vacuum. Compound **9** was finally recovered as fine white powder and was used without further purification (960 mg, yield 86%).^{1}H NMR (DMSO d_6, 250 MHz) δ (ppm): 8.76 (s, 2H, H-6, H-6″), 8.57 (d, $J = 7.8$ Hz, 2H, H-3, H-3″), 8.40 (d, $J = 7.5$ Hz, 2H, H-3′, H-5′), 8.05 (m, $J = 7.8$, 8.2, 6.7 Hz, 3H, H-4, H-4′, H-4″), 7.94 (s, 4H, OH), 4.66 (s, 2H, –CH, imid), 1.09 (d, $J = 6.6$ Hz, 24H, $-CH_3$, imid). ^{13}C NMR (DMSO d_6, 63 MHz, δ ppm): 154.5, 153.9, 148.9, 137.2, 136.6, 129.1, 120.0, 119.4, 87.5, 65.8, 23.9, 16.8. MS FAB (NBA matrix) m/z 549.4 (100%)$(M+H)^+$, calculated (MW) 549.66. UV–Vis (DMSO) λ_{max} (ε, $mol^{-1}cm^{-1}$) 290 nm (11 900). FT-IR (KBr pellet, ν cm^{-1}) 3252 (s, broad, ν_{OH}), 2988 (s,ν_{C-Hal}), 2930 (s, ν_{C-Hal}), 1596 (m, pyr), 1560 (m, pyr), 1374 (s), 1262 (s, pyr). Elemental analysis Calc. for $C_{29}H_{39}N_7O_4\cdot 2H_2O$: C 59.50%, H 7.35%, N 16.75%, C/N = 3.55; Found: C 59.4%, H 7.55%, N 16.63%, C/N = 3.57. It decomposes before melting at 186–187 °C.

2.10. Synthesis of 5,5″-Bis(1-oxyl-3-oxo-4,4,5,5-tetramethylimidazolidin-2-yl)2,2′:6′,2″-terpyridine (*10*) (diNN-Terpy)

The 5,5″-Bis(1,3-dihydroxy-4,4,5,5-tetramethylimidazolidin-2-yl)2,2′:6′,2″-terpyridine (**9**, 217 mg, 0.39 mmol) was charged into a small flask together with 20 ml of $CHCl_3$ and CH_2Cl_2 (4/1). Then it was degassed and kept under argon while stirring at room temperature. Separately, a solution of $NaIO_4$ (211 mg, 0.987 mmol) dissolved in 10 ml of H_2O was first degassed and saturated by argon exchange; then it was added to the solution of **9** by using a syringe under argon. After 30 min a deep green solution was obtained. The organic layer was extracted by using portions of $CHCl_3$ (3 × 10 ml) until the aqueous phase was almost colorless. The organic solution was evaporated by continuous argon bubbling till small volume. The mixture was separated by column chromatography (Aluminium oxide, acetone/light petroleum ether, 3/7). The 5,5″-Bis(1-oxyl-3-oxo-4,4,5,5-tetramethylimidazolidin-2-yl)2,2′:6′,2″-terpyridine (**10**) (diNN-Terpy) ($R_f = 0.23$) was obtained after solvent evaporation (by argon bubbling) as deep green powder (35 mg, yield 16%). FT-IR (KBr pellet, ν cm^{-1}): 3066 (w, ν_{C-Har}), 2990 (m, ν_{C-Hal}), 2924 (m, ν_{C-Hal}), 2853 (m, ν_{C-Hal}), 1591 (m, pyr), 1482 (m, pyr), 1452 (m, pyr), 1387 (m), 1351 (s, N–O), 1216 (m, pyr). MS FAB (NBA matrix) m/z 544.6 (100%) $[M+H]^+$, calculated (MW+H, 544.66). UV–Vis ($CHCl_3$) λ_{max} (ε, $mol^{-1}cm^{-1}$) 718 (145), 650 (425), 605 nm (480), 562 (350), 387 nm (13100), 342 nm (28 300), 328 nm (33 400), 282 nm (31 550).

2.11. Synthesis of 5,5″-Bis(1-oxyl-4,4,5,5-tetramethylimidazolidin-2-yl)2,2′:6′,2″-terpyridine (*11*)

The 5,5″-Bis(1,3-dihydroxy-4,4,5,5-tetramethylimidazolidin-2-yl)2,2′:6′,2″-terpyridine (**9**, 240 mg, 0.44 mmol) was charged into a small flask together with 20 ml of a mixture of $CHCl_3$ and CH_2Cl_2 (4/1), under stirring at room temperature. A solution of $NaIO_4$ (377 mg, 1.76 mmol, 10 ml H_2O) was slowly added to the solution of **9** and then the mixture was slightly warmed at 40 °C. After 30 min an orange–red solution was obtained. The organic layer was extracted by using portions of $CHCl_3$ (3 × 10 ml) until the aqueous phase was almost colorless. The organic solution was evaporated under reduced pressure till small volume. The mixture was separated by column chromatography (Aluminium oxide, acetone/light petroleum ether, 3/7). The 5,5″-Bis(1-oxyl-4,4,5,5-tetramethylimidazolidin-2-yl)2,2′:6′,2″-terpyridine (**11**) (diIN-Terpy) ($R_f = 0.25$) was obtained after solvent evaporation as orange powder (63 mg, yield 28%). FT-IR (KBR pellet, cm^{-1}): 3070 (w, ν_{C-Har}), 2957 (s, ν_{C-Hal}), 2924 (s, ν_{C-Hal}), 2870 (m, ν_{C-Hal}), 1596 (m, pyr), 1554 (s, C=N), 1469 (s, pyr), 1448 (s, pyr) 1425 (s), 1378 (s, N–O), 1262 (s, pyr), 1216 (s, pyr). MS FAB (NBA matrix) m/z 512.2 (100%) $[M+H]^+$, (calculated MW 511.6). UV–Vis ($CHCl_3$) λ_{max} (ε, $mol^{-1}cm^{-1}$) 528 (170), 490 (315), 459 nm (380), 300 nm (16 200), 257 nm (24 100).

3. Results and discussion

3.1. Synthetic procedures

Scheme 1 outlines the approach used for the synthesis of the key precursor 5,5″-diformyl-2,2′:6′,2″-terpyridine (**8**). Although **8** had been prepared previously [13] starting from 5,5″-dimethyl-2,2′:6′,2″-terpyridine, we decided to test a different route that leaves open further synthetic extensions. While this route implies a multistep synthesis, it offers in our opinion two advantages. First the intermediates (e.g. **2**, **3**, **7**, **8**) are easy to purify from the crude mixtures and second the novel compound **7** can further be utilized for asymmetric synthesis since it carries different functional groups (bromine and carbaldehyde). On the other hand the stannyl-compounds **4** and **6** were not isolated but rather used in situ [17]. The 2,5-dibromopyridine (**1**) can be selectively mono-lithiated in position 5 [14] using ether as reaction solvent. After quenching with DMF it gives the corresponding 6-bromo-3-pyridinecarbaldehyde (**2**) [15]. The protection of the carbaldehyde group in **2** was achieved

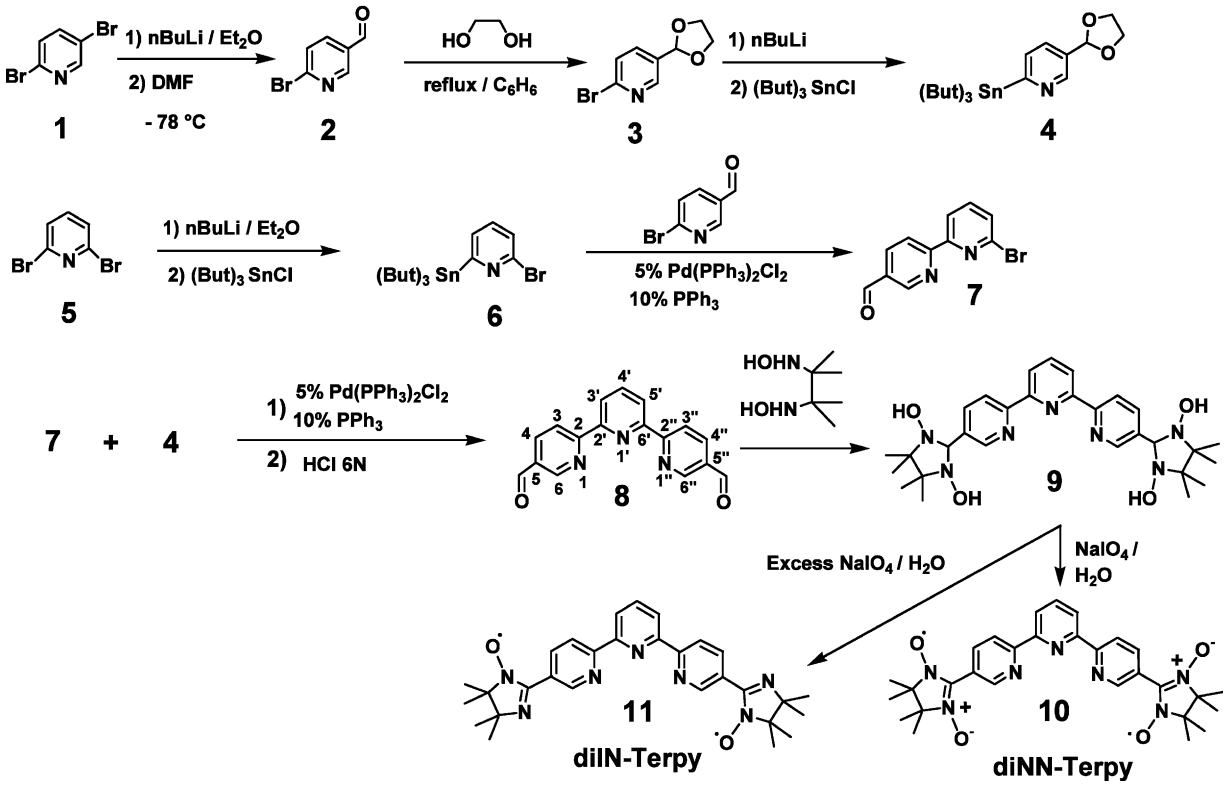

Scheme 1.

by formation of the correspondent 2-bromo-5-[1,3]dioxolan-2-yl-pyridine (**3**) using toluene-4-sulfonic-acid as catalyst ($CH_3C_6H_4SO_3H\cdot H_2O$, 8% mol) with ethyleneglycol.

Lithium exchange followed by quenching with Bu_3SnCl afforded 2-tributylstannyl-5-[1,3]dioxolan-2-yl-pyridine (**4**) used for Stille coupling reaction with compound **7**. 2,6-dibromopyridine (**5**) was initially mono-lithiated. The subsequent quenching with tributyltin-chloride (Bu_3SnCl) yielded 2-tributylstannyl-6-bromopyridine (**6**) as pale yellowish oil. Stille coupling with 6-bromo-3-pyridinecarbaldehyde (**2**) in anhydrous toluene under argon gave 6-bromo-2,2′-dipyridine-5′-carbaldehyde (**7**). The optimized conditions obtained for the coupling between **2** and **6** were achieved by using excess of **2** (2.4 equiv.) with respect to **6** (1 equiv.) together with $Pd(PPh_3)_2Cl_2$ (5% mol) and PPh_3 (10% mol) as catalyst. The Stille coupling reaction between **4** and **7** in degassed toluene under argon was carried out in a similar way as for **2** and **6** by heating to reflux for 60 h; further hydrolysis of the dioxolane in the presence of HCl (6 N) followed by basification gave 5,5″-diformyl-2,2′:6′,2″-terpyridine (**8**). The diformyl derivative **8** (1 equiv.) was then subjected to Ullman coupling with 2,3-bis-hydroxylamino-2,3-dimethyl-butane (3 equiv.) using a mixture of 1,4-dioxane, trichloromethane and methanol (4/3/3) as solvents for 7 days, under argon at room temperature. The white precipitate 5,5″-Bis(1,3-dihydroxy-4,4,5,5-tetramethylimidazolidin-2-yl)2,2′:6′,2″-terpyridine (**9**) formed was oxidized at room temperature, working under phase transfer conditions ($CHCl_3$/CH_2Cl_2/H_20), by using slight excess of $NaIO_4$ (2.5 equiv.) with respect to **9** (1.0 equiv.) for 30 min. After column chromatography 5,5″-Bis(1-oxyl-3-oxo-4,4,5,5-tetramethylimidazolidin-2-yl)2,2′:6′,2″-terpyridine (**10**) (diNN-Terpy) was obtained as deep-green powder. Similarly but using an excess of $NaIO_4$ (4 equiv.) with respect to **9** (1.0 equiv.) and warming the mixture up to 40 °C, the 5,5″-Bis(1-oxyl-4,4,5,5-tetramethylimidazolidin-2-yl)2,2′:6′,2″-terpyridine (**11**) (diIN-Terpy) was obtained as orange–red powder. The biradicals **10** and **11**, as expected, are relatively stable as powder over several months. In protic solvents (e.g. CH_2Cl_2 or $CHCl_3$) we observe a clear decrease of their stability upon prolonged storage.

3.2. Optical properties

In Fig. 1, we report for comparison the infrared spectra of the precursor 5,5″-Bis(1,3-dihydroxy-4,4,5,5-tetramethylimidazolidin-2-yl)2,2′:6′,2″-terpyridine (**9**) (Fig. 1(A)), the diNN-Terpy radical **10** (Fig. 1(B) and the diIN-Terpy radical **11** (Fig. 1(C)). Upon oxidation the strong signal around 3252 cm^{-1} for **9** originating by the OH stretching-mode disappears in **10** and **11** being accompanied, in the case of **10**, by an unusually strong signal at 1351 cm^{-1}. This was assumed to arise from the N–O stretching mode as described in other work for a

similar terpyridine system [6b] (4,4″-Bis(1,3-dihydroxy-4,4,5,5-tetramethylimidazolidin-2-yl)2,2′:6′,2″-terpyridine). In the case of **11** the novel signal, absent in **9**, is shifted to longer wavenumbers (1378 cm^{-1}) being accompanied by the appearance of a strong signal at 1554 cm^{-1} that may be tentatively attributed to the C=N stretching mode. The UV–Vis spectra of **10** and **11** are shown in Fig. 2. The diNN-Terpy radical **10** displays an intense blue color (λ_{max} 605 nm, $\varepsilon = 480\ M^{-1}\ cm^{-1}$) while the diIN-Terpy radical **11** manifests the typical bright orange–red color (λ_{max} 459 nm, $\varepsilon = 380\ M^{-1}\ cm^{-1}$).

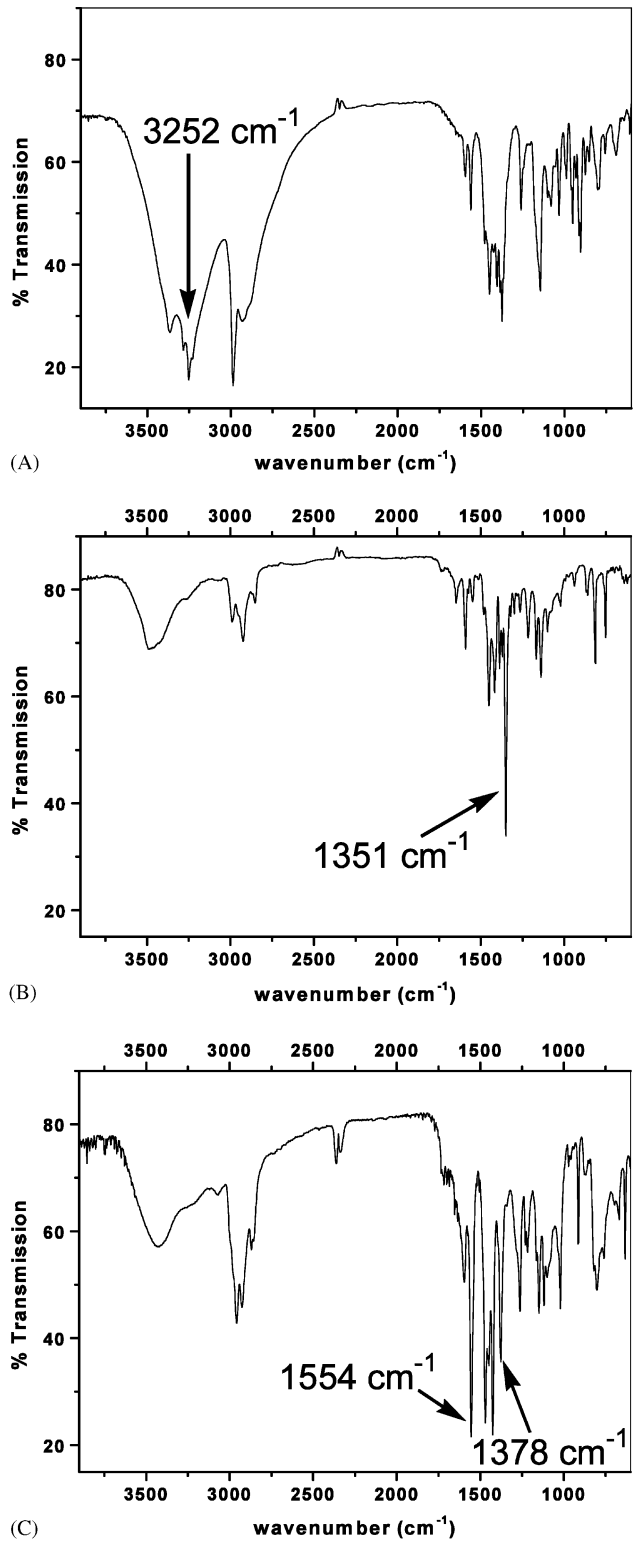

Fig. 1. FT-IR spectra of the precursor (A) 5,5″-Bis(1,3-dihydroxy-4,4,5,5-tetramethylimidazolidin-2-yl)2,2′:6′,2″-terpyridine (**9**), (B) diNN-Terpy (**10**) and (C) diIN-Terpy (**11**).

3.3. EPR spectra in solution

The EPR spectra of diNN-Terpy (**10**) and diIN-Terpy (**11**) are better resolved in diluted toluene solution [1×10^{-4} M] rather than in chloroform or dichloromethane and are shown in Fig. 3(A) and (B) respectively. The diNN-Terpy (**10**) displays a well resolved nine line pattern (Fig. 3(A)) demonstrating that the intramolecular exchange interaction between the two radical fragments is larger than the hyperfine terms ($J/a_N \gg 1$, i.e. $J \gg 7 \times 10^{-4}\ cm^{-1}$) [18]. Thus the observed line spacing (apparent hyperfine interaction, a_N) corresponds to half of that observed for the relative monoradical (where $a_N = 0.748$ mT). The spectrum is well reproduced by assuming the apparent hyperfine interaction $a_N = 0.374$ mT with four nitrogen nuclei, an average g value, $g_{iso} = 2.0066$, pure Lorentzian line-shape for the single components and peak-to-peak line width, $\Delta B_{pp} = 0.135$ mT. Similarly, strong exchange-interaction between the radical fragments is observed for diIN-Terpy (**11**) (Fig. 3(B)). The spectrum is reproduced by assuming the strong exchange limit ($J/a_N \gg 1$, i.e. $J \gg 4.2 \times 10^{-4}\ cm^{-1}$) with the following parameters, $a_{N1} = 0.430$ mT, $a_{N2} = 0.225$ mT, $g_{iso} = 2.0061$, the Lorentzian/Gaussian line-shape of 1/3 and the peak-to-peak line width, $\Delta B_{pp} = 0.200$ mT. Both, diNN-Terpy (**10**) and diIN-Terpy (**11**), displayed Curie-like behavior (inset Fig. 3(A) and (B) respectively) within the range 300–210 K,

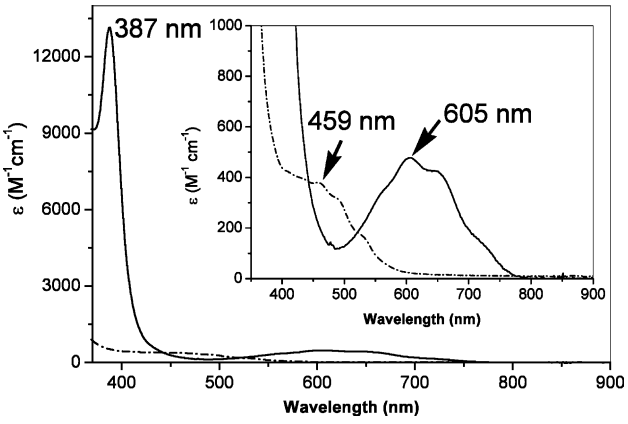

Fig. 2. UV–Vis spectra of diNN-Terpy (**10**) (plain line) and diIN-Terpy (**11**) (dashed line) in $CHCl_3$. The inset shows magnified the visible region of the spectra.

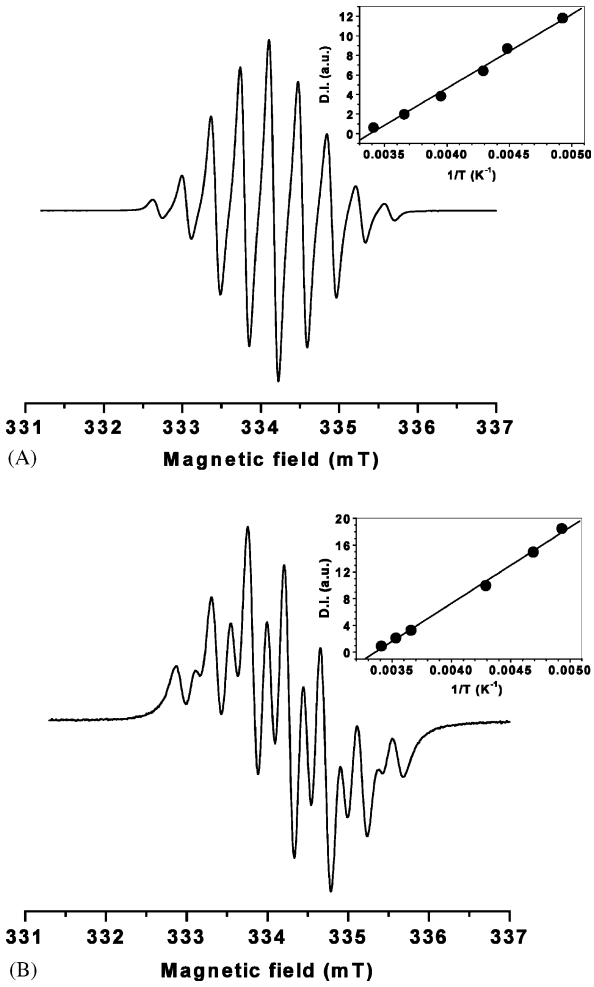

Fig. 3. EPR spectra of (A) diNN-Terpy (**10**) and (B) diIN-Terpy (**11**). Parameters for (A): frequency 9.400220 GHz, 100 KHz mod. frequency, 0.3 Gauss modulation amplitude, 21 ms time constant, 42 s sweep time, 2.6 mW microwave power, 10^5 gain, temperature 260 K, 6 scan were accumulated and averaged. The inset shows the correspondent Curie behavior. Parameters for (B): frequency 9.402404 GHz, 100 KHz mod. frequency, 0.3 Gauss modulation amplitude, 21 ms time constant, 42 s sweep time, 5.0 mW microwave power, 4×10^4 gain, temperature 260 K, 4 scan were accumulated and averaged. The inset shows the correspondent Curie behavior.

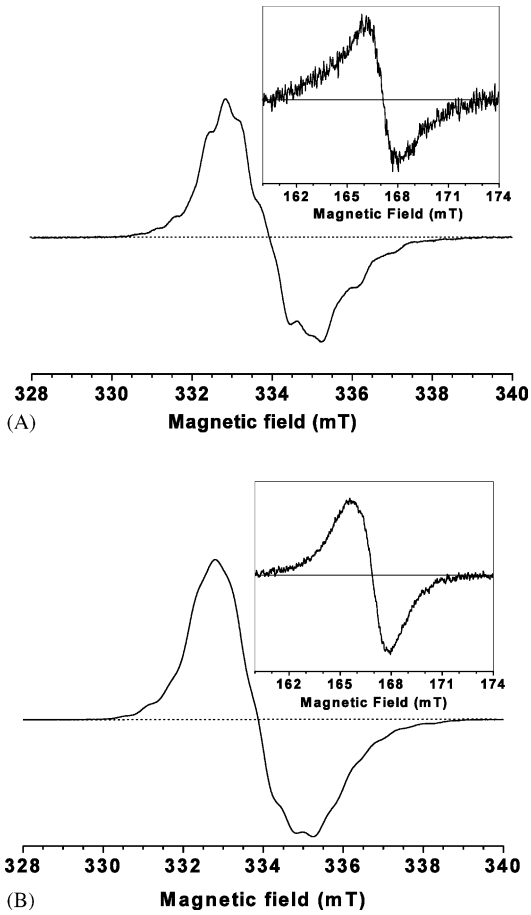

Fig. 4. EPR spectra of (A) diNN-Terpy (**10**) and (B) diIN-Terpy (**11**) in frozen solution. Parameters for (A): frequency 9.400712 GHz, 100 KHz mod. frequency, 0.6 Gauss modulation amplitude, 42 ms time constant, 84 s sweep time, 0.8 mW microwave power, 10^4 gain, temperature 110 K, 4 scan were accumulated and averaged. The inset shows the correspondent $\Delta m_s = 2$ transition. Parameters: 44 s sweep time, 84 ms time constant, 4.0 Gauss modulation amplitude, 32 mW microwave power, 24 scans were accumulated and averaged. Parameters for (B): Frequency 9.39697 GHz, 100 KHz mod. frequency, 0.6 Gauss modulation amplitude, 42 ms time constant, 84 s sweep time, 0.8 mW microwave power, 10^4 gain, temperature 110 K, 4 scan were accumulated and averaged. The inset shows the correspondent $\Delta m_s = 2$ transition. Parameters: 44 s sweep time, 84 ms time constant, 4.0 Gauss modulation amplitude, 32 mW microwave power, 30 scans were accumulated and averaged.

with the linear increase of the double-integrated signal intensities upon lowering the temperature. Furthermore, only a slight increase in the peak-to-peak line width was observed for **10** and **11** upon cooling.

3.4. EPR spectra in frozen solution

The EPR spectrum of the allowed transitions ($\Delta m_s \pm 1$) for diNN-Terpy **(10)** (toluene, 4×10^{-4} M) measured at 110 K is shown in Fig. 4(A). The observed spectrum accounts for the following spin-*Hamiltonian* in the case of a biradical system

$$H = \mu_B \mathbf{S} g \mathbf{B} + D\{S_z^2 - S(S+1)/3\} + E(S_x^2 - S_y^2)$$

where μ_B, g and B are respectively Bohr magneton, g-tensor and static magnetic field while the $|D|$ and $|E|$ terms represent the fine structure parameters (axial and rhombic). It is clear from the spectrum, although part of the anisotropic pattern is retained, that most of the hyperfine couplings are not resolved. This arises from dipolar interactions characteristic of randomly oriented triplet species. The computer simulation is not straightforward since it implies the knowledge of several parameters such as the hyperfine tensor of N nuclei (not included in the spin-Hamiltonian equation reported above) and the anisotropic g tensor; in addition, several conformers with slightly different parameters have probably to be taken into account. Thus its complete

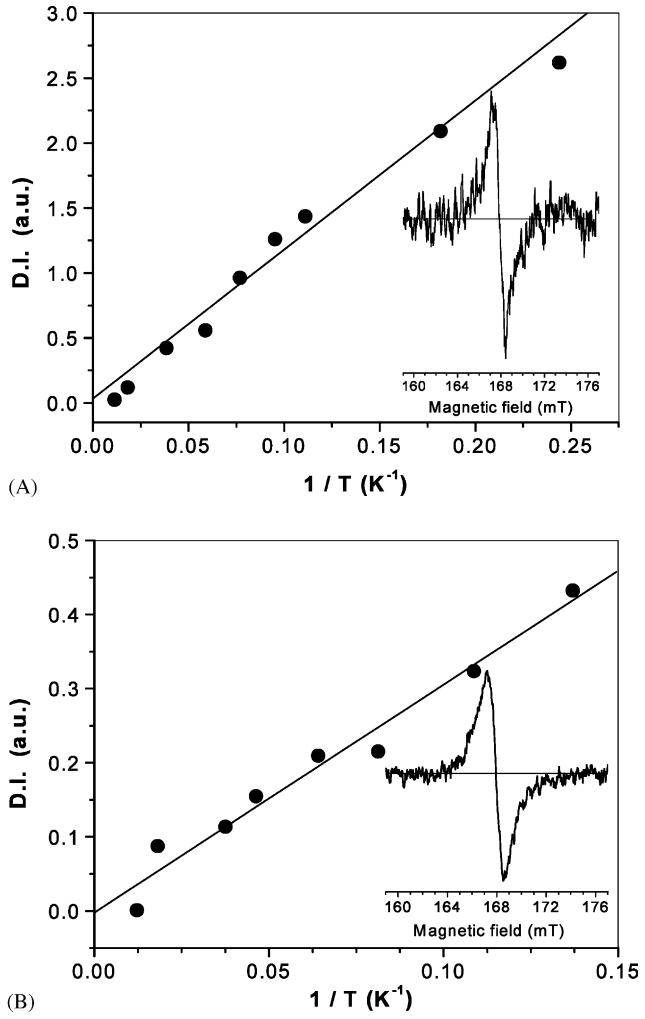

Fig. 5. Curie-law behavior for (A) diNN-Terpy (**10**) and (B) diIN-Terpy (**11**) at cryogenic temperature. The respective inset shows the $\Delta m_s = 2$ transition for **10** (A, 9.4463 GHz, $T = 4.1$ K, 5 scan, 80 μW) and **11** (B, 9.4427 GHz, $T = 7.3$ K, 5 scan, 320 μW), 42 s sweep time, 164 ms time constant, 10^6 gain, 100 KHz modulation frequency, 4.0 Gauss modulation amplitude.

simulation has not been achieved. However, the spectrum accounts for $g_{av} = 2.0066$ with the estimated $|D/hc| = 3.46 \times 10^{-3}$ cm^{-1}. Assuming the point-dipole approximation, the D' ($D' = |D/hc|$) value is consistent with the mean distance between the centers of the ONCNO groups of ~9.1 Å. The biradical nature of diNN-Terpy (**10**) was further confirmed by the appearance of the forbidden transition at half-field ($\Delta m_s \pm 2$, $g_{av} = 4.01$, inset Fig. 4(A)). The EPR spectrum of the allowed transitions ($\Delta m_s \pm 1$) for diIN-Terpy (**11**) (toluene, 6×10^{-4} M) measured at 110 K is shown in Fig. 4(B). It displays an even more 'isotropic' pattern with respect to that one shown by diNN-Terpy (**10**), with the average g value, $g_{av} = 2.0061$, and the estimated $D' = 3.69 \times 10^{-3}$ cm^{-1} consistent with a mean distance between the centers of the ONCN groups of ~8.9 Å. In harmony with the results from **10**, the appearance of the forbidden transition at half-field ($\Delta m_s \pm 2$, $g_{av} = 4.01$, inset Fig. 4(B)) ensures the biradical nature of **11**. In order to access the trend in the magnetic properties of the isolated radicals, the temperature dependence of the $\Delta m_s = 2$ transitions for **10** and **11** [solutions of 10^{-3} M in toluene] was further followed at cryogenic temperature. The double integrated signal intensities of **10** and **11** are shown in Fig. 5(A) and (B), respectively. The microwave power applied in the measurements was kept in such a way that the signal intensities were proportional to the square root of the power. The linear increase of the signal (D.I) versus the inverse temperature (K^{-1}) was observed in both cases, according to the Curie law. Consequently, there is no thermal population or depopulation of the spin state of the molecules within the examined temperature range. On the other hand, the interpretation of the present results is not straightforward enough for clear attribution of the ground spin state of **10** and **11**. Either the triplet state ($S = 1$) is the lowest-energy state separated from the singlet ($S = 0$) by a substantial gap relative to the thermal energy ($|2J| > K_bT$), or the energy difference between triplet ($S = 1$) and singlet ($S = 0$) is extremely small leading to degeneracy of those levels. In this case any changes in temperature do not shift the thermal equilibrium between the two states and thus they are statistically populated according to the Boltzmann distribution ($\exp -[\Delta E/K_bT]$). In order to further support ground state multiplicity, the singlet–triplet gap was then considered theoretically.

3.5. Theoretical calculations

Quantum chemical calculations were performed in order to predict theoretically the ground spin-state of the target biradicals. The singlet–triplet splitting:

$$\Delta E_{ST} = E_S - E_T = 2J \quad (1)$$

and the spin density distribution of biradicals **10** and **11** were determined. In Eq. (1) E_S and E_T are the calculated energies of the lowest singlet and triplet states respectively and J is the exchange integral. The geometry of the biradicals was optimised both with UHF/AM1 and

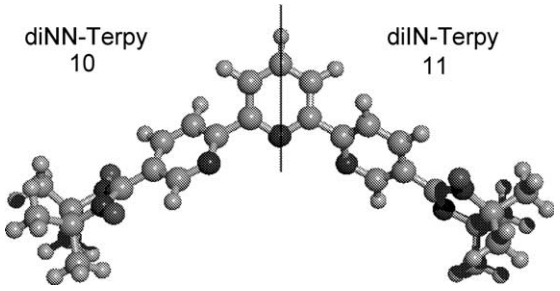

Fig. 6. ROHF/AM1 optimised triplet state geometry of biradicals **10** (left) and **11** (right).

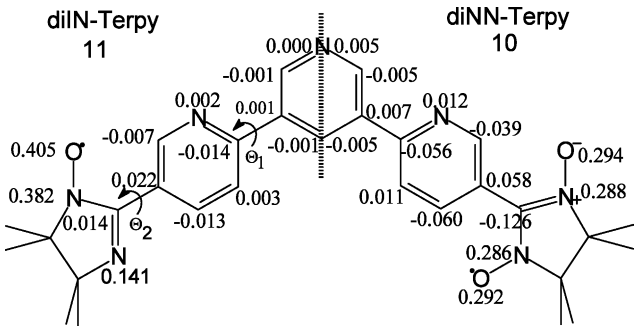

Fig. 7. ROHF/AM1/CIS(20,20) calculated spin densities of conformation **b** of biradicals **10** (right) and **11** (left).

ROHF/AM1, the two methods yielding virtually identical lowest energy structures. Furthermore, no essential differences were witnessed between the geometry of the unrestricted singlet and triplet molecules. Therefore, the ROHF/AM1 structures of **10** and **11** (see Fig. 6) were used further on for calculation of the spin-state energies. The imino nitroxide and the nitronyl niroxide rings are essentially planar (intraring torsion angles $\leq 10^{\circ}$), with the N–O bonds about 15° out of the ring plane. The calculated bond lengths fall within the range of those measured for radicals of this class [23]. The N–O bonds are slightly shorter than the most commonly encountered experimental value of 1.28 Å, namely $R_{N-O} =$ 1.209 and 1.204 for **10** and **11**, respectively. This result is similar to previous AM1 calculations [23b]. An interesting structural feature of the molecules are the torsional angles Θ_1 and Θ_2 (see Fig. 7 for notations). They reflect the possibility for free rotation around the two single bonds and hence can be a measure for the effective π-conjugation through the spacer. This is directly related to the intramolecular exchange coupling of the two radical moieties. Therefore, a conformational search, i.e. systematic variation of Θ_1 and Θ_2 with calculation of the corresponding energy, was performed at the UHF/AM1 level. 92% of the conformations of **10** and 100% of those of **11** differ in energy by less than 5 kcal mol^{-1}. This result indicates relatively high flexibility of the two molecules, the rotation barrier being lower in **11** than in **10**. The calculated singlet–triplet splitting and heats of formation of **10** and **11** are collected in Table 1. The simulations predict triplet ground state for both biradicals evidenced by the

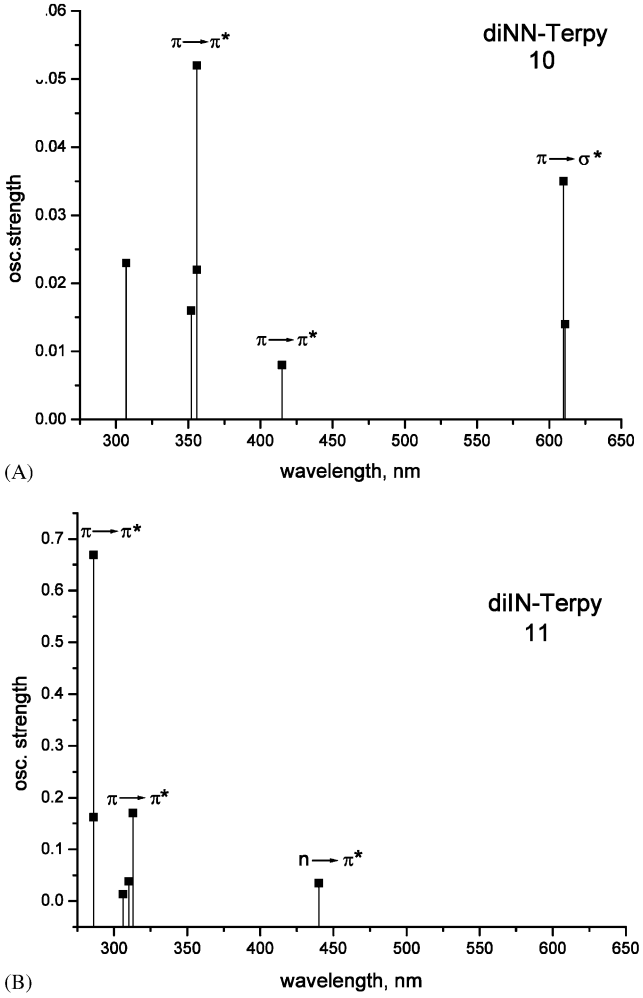

Fig. 8. ROHF/AM1/CIS [20,20] calculated absorption spectra of **10** (A) and **11** (B).

positive values of ΔE_{ST}. The triplet state is more stable with respect to the singlet in **10** than in **11**, which is probably due to more effective π-conjugation resulting from the less flexible structure of **10**. It is apparent that the exchange coupling is extremely sensitive to rotation around the single bonds. Increase of Θ_1 to $\sim 90^{\circ}$ results in practically degenerate singlet and triplet states. This is an indication for hampered intramolecular coupling between the radical sites due to prevented spin transfer into the spacer. The calculated spin densities are presented in Fig. 7 as an additional illustration. Both

Table 1
ROHF/AM1/CAS [8,8] calculated singlet–triplet gap (ΔE_{ST}) and heat of formation (H_f) of biradicals **10** and **11** for different torsions Θ_1 and Θ_2

Radical	Conformation	Θ_1 °	Θ_2 °	ΔE_{ST}, kcal mol^{-1}	H_f, kcal mol^{-1}
10	a	86	0	0.0006	192.898
	b	49	27	0.2499	195.846
11	a	84	7	0.0000	188.968
	b	47	20	0.0269	192.376

biradicals feature alternating signs of the spin densities at neighbouring atoms throughout the whole molecule. Thus, the main topological prerequisite for effective ferromagnetic exchange coupling is fulfilled. Increase of Θ_1 to $\sim 80^\circ$ (conformation **a** in Table 1) leads to zero value of the spin density at the carbon sites connecting the central pyridine ring to the two outer ones. A direct consequence is the inability for spin transfer and hence a breakdown in spin polarization. Although conformation **a** has slightly lower heat of formation in the gas phase, the small rotation barrier allows stabilization of more planarised structure like **b**. We have also used the ROHF/AM1/CIS approach to simulate the absorption spectra of the two biradicals. This would verify the applicability of the computational procedure for theoretical prediction of the absorption spectra of similar compounds and furthermore allow assignment of the type of the observed experimental transitions. The calculated absorption spectra are depicted in Fig. 8. The predicted transition wavelengths correspond fairly well to the experimental values. The longest wavelength transitions in both **10** and **11** originate from the radical. In **11** this is an $n \rightarrow \pi^*$ transition at 440 nm from the radical SOMO to an anti-bonding π^* MO. In **10**, however, there are two degenerate transitions (at 611 and 610 nm) between the radical HOMO and one of its anti-bonding σ^*-type MOs. Unexpectedly, these two transitions are rather intensive. The second characteristic transition for nitronyl nitroxide (at 415 nm) is reproduced as well. However, the predicted wavelength is higher than the experimental value of 387 nm. The calculated $\pi \rightarrow \pi^*$ transitions arising from the terpyridine core follow a reasonable trend. The wavelength in **11** (286 nm) corresponds to the one measured for pure terpyridine [23]. A bathochromic shift of ~ 70 nm is observed in **10** due to the enhanced conjugation. This is also in line with the experimentally measured spectra.

4. Conclusion

The novel nitronyl nitroxide (**10**) and imino nitroxide (**11**) radicals attached to terpyridine spacer are synthesized. Both molecules show strong ferromagnetic-exchange interaction between the radical units as judged from the EPR analyses. Those represent the first example of ferromagnetically coupled Ullman radicals attached on terpyridine moieties reported so far. The double integrated signal intensities of the EPR absorption follow Curie-like behaviour for the $\Delta m_s = 2$ transition down to 4.1 K (**10**) and 7.3 K (**11**) as lowest temperatures respectively. The singlet–triplet splitting and the spin distribution of **10** and **11** are estimated theoretically. The triplet-ground state is predicted for both biradicals, in agreement with the topological models. The presented biradicals are considered as suitable ligands for further metal complexation for extended spin network.

Acknowledgements

The authors thank the DFG and the Marie-Curie Foundation (A.I.) for financial support.

References

[1a] G. Chelucci, R.P. Thummel, Chem. Rev. 102 (2002) 3129.
[1b] A.M.W. Cargill Thompson, Coord. Chem. Rev. 160 (1997) 1.
[1c] U. Lehmann, O. Henze, A.D. Schlüter, Chem. Eur. J 5 (1999) 854.
[2] (a) J.P. Sauvage, J.P. Collin, J.C. Chambron, S. Guillerez, C. Coudret, V. Balzani, F. Barigelletti, L. De Cola, L. Flamigni, Chem. Rev. 94 (1994) 993;
(b) J.-M. Lehn, Supramolecular Chemistry. Concepts and Perspectives, Wiley VCH, Weinheim, Germany, 1995.
[3] B.N. Trawick, A.T. Daniher, J.K. Bashkin, Chem. Rev. 98 (1998) 939.
[4] A. Harriman, R. Ziessel, Coord. Chem. Rev. 171 (1998) 331.
[5] E. Coronado, P. Delhaés, D. Gatteschi, J.S. Miller (Eds.), "Molecular Magnetism: From Molecular Assemblies to the Devices, NATO ASI Series E 321, Kluwer Academic Publishers, Dordrecht 1996.
[6] (a) M.A. Halcrow, E.K. Brechin, E.J.L. McInnes, F.E. Mabbs, J.E. Davies, J. Chem. Soc., Dalton Trans. (1998) 2477;
(b) C. Stroh, R. Ziessel, Tetrahedron Lett. 40 (1999) 4543;
(c) C. Stroh, P. Turek, P. Rabu, R. Ziessel, Inorg. Chem. 40 (2001) 5334.
[7] J.H. Osiecki, E.F. Ullman, J. Am. Chem. Soc. 90 (1968) 1078.
[8] (a) M. Kinoshita, Jap. J. Appl. Phys. 33 (1994) 5718;
(b) M. Deumal, J. Cirujeda, J. Veciana, Jap. J. Novoa. Adv. Mater. 10 (1998) 1461.
[9] (a) O. Kahn (Ed.), Magnetism: A Supramolecular Function, Kluwer, Dordrecht, 1996;
(b) J.S. Miller, M. Drillon, MagnetoScience: Molecules to Materials, Wiley-VCH, Weinheim, 2000.
[10] (a) M. Tamura, Y. Nakasawa, D. Shiomi, K. Nozawa, Y. Hosokoshi, M. Ishikawa, M. Takahashi, M. Kinoshita, Chem. Phys. Lett. 186 (1991) 401;
(b) Y. Nakazawa, M. Tamura, N. Shirakawa, D. Shiomi, N. Takahashi, M. Kinoshita, M. Ishikawa, Phys. Rev. B 46 (1992) 8906.
[11] (a) H.C. Longuet-Higgins, J. Chem. Phys. 18 (1950) 265;
(b) H.M. McConnell, J. Chem. Phys 39 (1963) 1916;
(c) W.T. Borden, E.R. Davidson, J. Am. Chem. Soc. 99 (1977) 4587;
(d) A.A. Ovchinnikov, Theor. Chim. Acta 47 (1978) 297;
(e) P.M. Lahti, Magnetic Properties of Organic Materials, Marcel Dekker, New York, 1999.
[12] (a) F.H. Burstall, J. Chem. Soc. 1938.;
(b) A.A. Schilt, G.F. Smith, Anal. Chim. Acta 15 (1956) 567;
(c) J.R. Kirchhoff, D.R. McMillon, P.A. Marnot, J.-P. Sauvage, J. Am. Chem. Soc. 107 (1985) 1138;
(d) J.-P. Sauvage, M. Ward, Inorg. Chem. 30 (1991) 3869;
(e) G.R. Newkome, D.C. Hager, G.E. Kiefer, J. Org. Chem. 51 (1986) 850;
(f) E.C. Constable, J.M. Holmes, R.C.S. McQueen, J. Chem. Soc., Dalton Trans. 5 (1987);

(g) Y. Uchida, M. Okabe, H. Kobayashi, S. Oae, Synthesis (1995) 939.
[13] I. Sasaki, J.C. Daran, G.G.A. Balavoine, Synthesis 5 (1999) 815.
[14] X. Wang, P. Rabbat, P. O'Shea, R. Tiller, E.J.J. Grabowski, P.J. Reider, Tetrahedron Lett. 41 (2000) 4335.
[15] F.J. Romero-Salguero, J.-M. Lehn, Tetrahedron Lett. 40 (1999) 859.
[16] D. Cai, D.L. Hughes, T.R. Verhoeven, Tetrahedron Lett. 37 (1996) 2537.
[17] For the toxicity of stannyl compounds see for example: A.G. Davies, P.J. Smith, Comprehensive Organometallic Chemistry In: E.W. Abel (Ed.) Pergamon, Oxford 2 (1982) 608.
[18] J.E. Wertz, J.R. Bolton, Electron Spin Resonance, Elementary Theory and Practical Applications, Chapman & Hall, 1986, p. 250.
[19] Selected data for [2,2′]-dipyridinyl-5-5′-dicarboxaldehyde: ^{1}H NMR (DMSO d_6, 250 MHz) δ (ppm): 10.26 δ (s, 2H), 9.31 δ (s, 2H), 8.75 δ (d, $J = 8.2$ Hz, 2H), 8.52 δ (dd, $J = 2.0$, 8.0 Hz, 2H).
[20] V.I. Ovcharenko, S.V. Fokin, G.V. Romanenko, I.V. Korobkov, P. Rey, Russ. Chem. Bull. 8 (1999) 1519.
[21] J.J.P. Stewart, MOPAC: A General Molecular Orbital Package (Version 7.2), QCPE, 1995.
[22] S. Karabunarliev, M. Baumgarten, K. Mullen, J. Phys. Chem. A 102 (1998) 7029.
[23] (a) R. Akabane, M. Tanaka, K. Matsuo, N. Koga, K. Matsuda, H. Iwamura, J. Org. Chem. 62 (1997) 8854;
(b) L. Zhang, Z. Liu, L. Wenig, D. Liao, Z. Jiang, S. Yan, P. Shen, M. Baumgarten, Helv. Chim. Acta 84 (2001) 834;
(c) K. Nakamoto, J. Phys. Chem. 64 (1960) 1420.
[24] P.M. Windscheif, F. Voegtle, Synthesis EN (1994) 87.